DETERMINATION OF THE DOPANT-RELATED BASE RESISTIVITY IN PRESENCE OF THERMAL DONORS

Juliane Broisch, Jonas Haunschild, Stefan Rein
Fraunhofer Institute for Solar Energy Systems
Heidenhofstr. 2, D-79110 Freiburg, Germany
Telephone: +49 761 4588 5271. Fax: +49 761 4588 5482. Juliane.Broisch@ise.fraunhofer.de

ABSTRACT: Thermal donors can form in Czochralski grown silicon during the cooling of the ingot. Base resistivity measurements in the as-cut state as well as the inline control of the emitter sheet resistance by inductive base resistivity measurements are influenced by these oxygen clusters. The influence of the thermal donors on the measurements results as well as on calculation results is quantified within this paper. Additionally, a new PL based method (PL-BR) for the determination of the dopant-related base resistivity despite the presence of thermal donors is presented. With the PL-BR method the dopant-related base resistivity and therefore the emitter sheet resistivity can be calculated with a significant higher accuracy than standard base resistivity measurements.
Keywords: base resistivity, Czochralsky silicon, thermal donors, PL-Imaging

1 INTRODUCTION

Due to the high oxygen content of Czochralski (Cz) silicon, thermal donors (TD) [1-5] may form during cooling of ingots in this silicon type. Base resistivity measurements by four-point-probe or inductive measurements in the as-cut state are influenced by these TD. Instead of the base resistivity related to the added dopants, a base resistivity depending on the sum of added dopants and TD is measured. During emitter diffusion or any other high temperature step within the solar cell process chain TD are annihilated. This aspect of the TD disturb the inline process control of the emitter sheet resistance, because this value is calculated from two inductive sheet resistivity measurements – one before and one after emitter formation [6].

To avoid these problems in process control we present a new method to determine the dopant-related base resistivity in the as-cut state. The method will be referred as "PL-BR" (PhotoLuminescence Base Resistivity). In Ref [7] was shown that TD form ring structures of varying resistivity, observable in PL images of wafers in the as-cut state which disappeared after TD annihilation. Fig. 1a-c show PL images in the as-cut state of three p-type samples with different shapes of ring patterns, in which the area with TD appear dark. In n-type silicon areas with TD appear brighter than the residual sample (see Fig. 1d). Due to the fact that these ring structures rarely cover the whole wafer, it should be possible to measure the dopant-related base resistivity at the outer corners of the wafer already in the as-cut state.

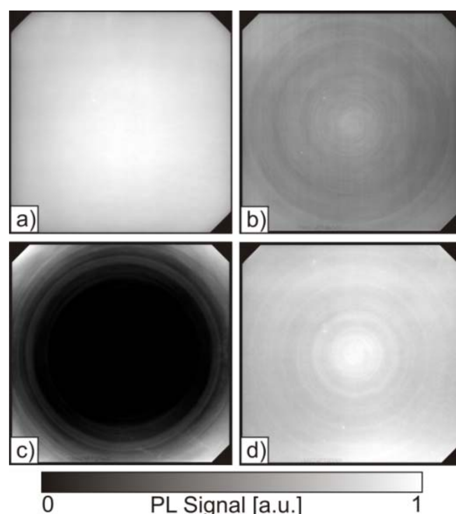

Fig. 1. PL images of as-cut Cz-Si samples with different shapes of ring patterns. a) p-type without ring pattern, b) p-type with medium ring pattern, c) p-type with dark ring pattern and d) n-type with inverted ring pattern.

2 INFLUENCE OF THERMAL DONORS ON BASE RESISTIVITY AND EMITTER SHEET RESISTANCE

2.1 Short summary on thermal donors

Thermal donors are clusters of oxygen atoms which associate in oxygen rich silicon during crystal cooling and which are negatively charged. During high-temperature steps these TD are dissociated or restructured so that the negative charges are neutralized. The formation of TD occurs in the temperature range between 300 °C and 500 °C [3, 5]. Several types of TD can form with different energy levels and single or double charges [8]. Since TD act as donors they influence the net-doping concentration and therefore the base resistivity. In p-type silicon the base resistivity increases due to TD and in n-type silicon the base resistivity decreases compared to the base resistivity value which is dopant-related. Above 500 °C the TD dissociate [3, 9-11]. But in the temperature range from 550 °C to 800 °C another type, the so called "new donors" (ND) can form, which can be eliminated above 850 °C. Therefore the best temperature for an annihilation of TD is > 850 °C [9].

2.2 Change of the base resistivity due to thermal donors

Since most thermal donors are eliminated during a high temperature step at temperatures higher than 550 °C [9-11], the change in base resistivity can be determined by resistivity measurements before and after thermal donor annihilation. For this investigation a representative set of p- and n-type samples was taken from inventory of Fraunhofer ISE PV-TEC [12]. The base resistivity was measured via four-point-probe measurement at a diagonal line scan for each investigated wafer. The mean values of the line scans before and after TD annihilation at 880 °C are displayed together with the standard deviations for the p-type and n-type wafers in Fig. 2 In addition, the difference between both measured base resistivities is shown in the lower graph of the figure.

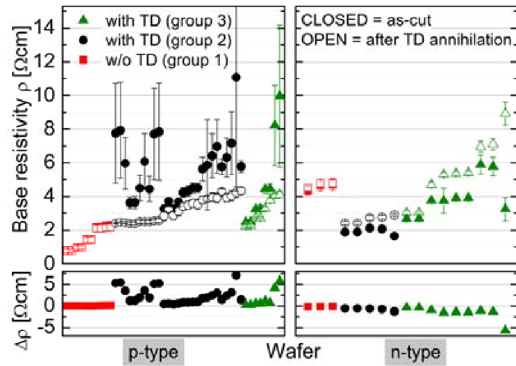

Fig. 2. (upper graph) Mean value of the base resistivity of each p- and n-type sample in the as-cut state (closed symbols) and after TD annihilation (open symbols). Samples without TD (group 1) are displayed with red squares, samples with TD are displayed with black circles (group 2) and with green triangles (group 3).
(lower graph) Difference of the base resistivity between the measurement before and after TD annihilation for each sample of the three groups.

Due to the negative charge of TD, the base resistivity of the p-type silicon decreases after TD annihilation due to the increase of the net doping concentration for most samples. Based on the change of the base resistivity and sample surface, the set of p-type samples was split into three groups: (1) wafers without TD and a rough surface in the as-cut state (red squares), (2) wafers with TD and a rough, slurry-cut surface in the as-cut state (black circles) and (3) wafers with TD and a smooth, diamond-cut surface in the as-cut state (green triangles). As can be seen from Fig. 2, the polishing of the surface after wafer sawing has no influence on the amount of TD. The only wafers without TD in this set of p-type samples have a base resistivity lower than 2 Ωcm.

In contrast to the p-type samples, the base resistivity of the n-type silicon increases due to the decrease of the net doping through the TD annihilation. The observed standard deviations in the as-cut state of the n-type samples are much smaller than for the p-type samples. Therefore the TDs seem to be distributed more homogeneous over the whole wafer than for the p-type samples or the amount of TD is lower than in p-type silicon. The set of n-type samples, which all have a rough surface, was also split into three groups: (1) wafers without TD in the as-cut state (red squares), (2) wafers with TD in the as-cut state whose resistivity value of the four-point-probe measurement at the corner region in the as-cut state is similar to the base resistivity value of the whole line scan after TD annihilation (black circles) and (3) wafers with TD in the as-cut state whose resistivity values of the four-point-probe measurement at the corner region in the as-cut state are lower than the base resistivity value of the whole line scan after TD annihilation (green triangles).

Diagonal line scans of a wafer from group 2 (solid lines) and group 3 (dashed lines) before and after TD annihilation are displayed in Fig. 3. The change of the resistivity curves due to TD annihilation is visible: Before TD annihilation the resistivity is lower in the middle of the sample than at the corners, while after TD annihilation the resistivity is nearly homogeneous over the whole sample. Since the phase interface during crystal pulling is bowed [13, 14], the whole wafer area does not crystallize at the same time and thus lateral difference in the dopant concentration exists.

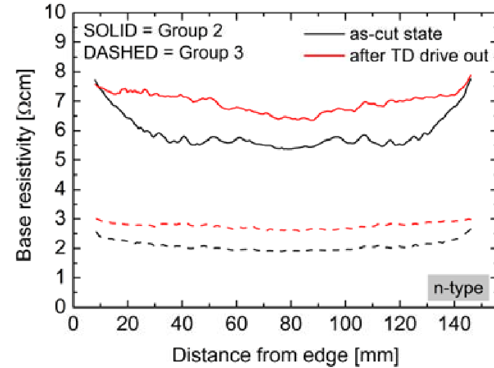

Fig. 3. Diagonal line scans of the base resistivity of two n-type Cz wafer in the as-cut state (black) and after TD annihilation (red).

2.3 Influence of the as-cut base resistivity on the calculation of the emitter sheet resistivity

For process control, the emitter sheet resistivity is calculated from an inductive resistivity measurement before and after emitter diffusion [6], because this technique determines the resistivity of the whole sample. The emitter sheet resistance R_{sh}^{E} is calculated from the base sheet resistivity R_{sh}^{B} and the total sheet resistivity of base plus emitter R_{sh}^{B+E} by the following equation:

$$R_{sh}^{E} = \frac{2R_{sh}^{B}R_{sh}^{B+E}}{R_{sh}^{B}-R_{sh}^{B+E}} \qquad (1)^{1}$$

Therefore, the calculated emitter sheet resistivity is influenced by deviations of the base resistivity due to TD, which is measured before emitter diffusion. To investigate this impact in more detail, a fixed value for the emitter sheet resistivity $R_{sh\text{-fixed}}^{E}$ is taken. With this fixed value the total sheet resistivity of base plus emitter $R_{sh-calc}^{B+E}$ can be calculated by solving equation (1). These calculations were done for different specific base resistivities ρ and wafer thicknesses W using:

$$\rho = R_{sh}^{B} \cdot W \qquad (2)$$

In a next step deviations ΔR_{sh}^{B} from the base resistivity value, which was used for the $R_{sh-calc}^{B+E}$ calculation, were defined by taking different percent of the used base resistivity value. Thereafter, the emitter sheet resistivity R_{sh}^{E} is calculated from $R_{sh-calc}^{B+E}$, R_{sh}^{B} and ΔR_{sh}^{B} by using the following equation based on equation (1):

$$R_{sh}^{E} = \frac{2(R_{sh}^{B}+\Delta R_{sh}^{B})R_{sh-calc}^{B+E}}{(R_{sh}^{B}+\Delta R_{sh}^{B})-R_{sh-calc}^{B+E}} \qquad (3)^{1}$$

Afterwards, the deviations of such calculated emitter sheet resistivities R_{sh}^{E} from $R_{sh\text{-fixed}}^{E}$ are calculated. These deviations are displayed in Fig. 4 as a function of ΔR_{sh}^{B} for $R_{sh\text{-fixed}}^{E}$ = 120 Ω/sq and W = 180 µm using different specific base resistivities in the typical range for solar cell production. The horizontal line marks a deviation of the calculated emitter sheet resistivity of 5 % from $R_{sh\text{-fixed}}^{E}$.

[1] Only valid for double-sided emitters. For a single-sided emitter the formula has to be divided by 2.

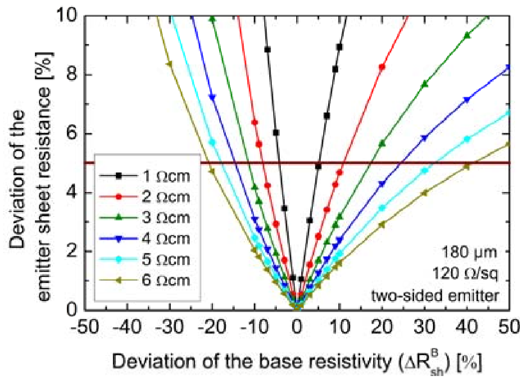

Fig. 4. Simulated deviation of the calculated emitter sheet resistance R^E_{sh} as a function of ΔR^B_{sh} for $R^E_{sh\text{-fixed}}$ = 120 Ω/sq and W = 180 µm. The horizontal red line marks a deviation of the emitter sheet resistance of 5 %.

Two observations are made from Fig. 4: i) The deviation of the emitter sheet resistance increases with decreasing base resistivity for the same value of ΔR^B_{sh}. ii) The deviation of the emitter sheet resistance is higher for negative values of ΔR^B_{sh} than for positive values. Therefore, if the dopant-related base resistivity and the value of ΔR^B_{sh} due to TD are similar, the deviation of the emitter sheet resistivity is higher for a p-type sample than for an n-type sample.

Fig. 5 compares the deviations of the calculated emitter sheet resistivity for two values of $R^E_{sh\text{-fixed}}$ (65 Ω/sq and 120 Ω/sq) for a fixed specific base resistivity of 1 Ωcm using different sample thicknesses *W* (160 µm and 180 µm) and different kinds of emitter (single-sided and double-sided).

The comparison shows that for thicker samples the calculated deviation of the emitter sheet resistance is higher (see red and black curves in Fig. 5) due to the relation between specific base resistivity and base sheet resistivity (eq. (2)). Furthermore, the deviation of the emitter sheet resistance is higher for a single-sided emitter (dashed lines with open symbols) than for a double-sided emitter (continuous lines with closed symbols). In addition, it is shown that an emitter with a lower sheet resistivity and therefore a higher doping concentration tolerates higher deviations of the as-cut base resistivity than an emitter with high values of the emitter sheet resistivity.

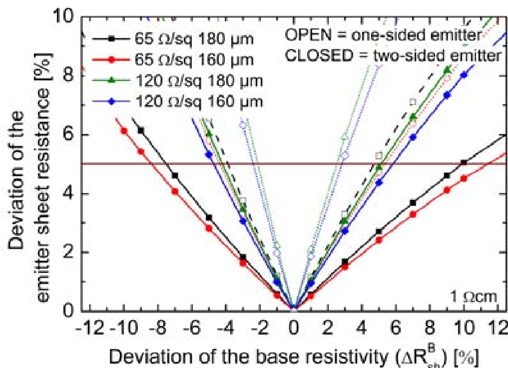

Fig. 5. Simulated deviation of the calculated emitter sheet resistance R^E_{sh} from $R^E_{sh\text{-fixed}}$ as a function of ΔR^B_{sh} for different values of $R^E_{sh\text{-fixed}}$ and wafer thicknesses W. Continuous lines with closed symbols represent the simulation for a double-sided emitter, while dashed lines with open symbols stand for a single-sided emitter. The horizontal red line marks a deviation of the emitter sheet resistance of 5 %.

In summary, the higher the targeted emitter sheet resistivity is, the lower the deviation of the base resistivity in the as-cut state from the dopant-related one has to be. Hence, to ensure that normally used emitter sheet resistivities up to 120 Ω/sq. are calculated with an accuracy of 5 % for wafers with a thickness of 180 µm and ρ >1 Ωcm, the deviation of the as-cut base resistivity has to be less than 5 % from the dopant-related value. But as TD have a stronger influence in most cases, a new method to determine the correct value of the base resistivity is needed.

3 DETERMINATION OF THE DOPANT-RELATED BASE RESISTIVITY IN THE AS-CUT STATE BY PL-IMAGING

3.1 Determination principle

The observation from Ref. [7] that ring structures disappear after thermal treatment is confirmed by a comparison of the PL image[2] of a wafer in the as-cut state and after TD annihilation (see Fig. 6). This observation suggests that the TD are the origin of the ring pattern. As the pattern does not cover the whole wafer, it should be possible to measure the dopant-related base resistivity already in the as-cut state at the corners of the wafer.

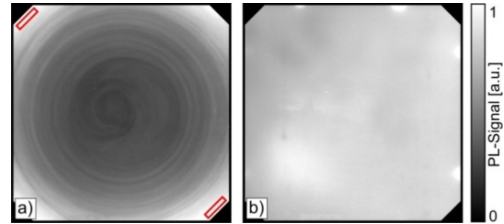

Fig. 6. PL images of a p-type Cz wafer (a) in the as-cut state and (b) after TD annihilation. The red rectangles mark the areas from which the PL signal was taken for resistivity determination.

This observation can be explained by the fact that TD form during crystal cooling and a crystal cools down from the outside to the crystal center and thus most of the TD are formed in the middle of crystal.

With a four-point-probe measurement tool it is possible to measure the sheet resistance with high resolution and accurate localization of the measurement points. Therefore, it is possible to measure the base resistivity in the as-cut state at the corners of a wafer, but without the exact information about the actual pattern of the ring structures, finding the exact position of the optimal point for a single-spot measurement is difficult. Since the ring structures can be observed easily by PL and since the PL intensity I_{PL} in low injection (see equation (4)) is dominated by the doping concentration of the material [16], it is possible to calibrate the PL signal directly to the base resistivity.

[2] For PL measurements the laser was widened to illuminate the whole wafer at once. More details about the used PL setup can be found in Ref. [15].

$$I_{PL} = A_i \cdot B \cdot \Delta n \cdot N_{netto} \, , \qquad (4)$$

with A_i a scaling factor, B the radiative recombination coefficient, Δn the excess minority carrier concentration and N_{netto} the net-doping concentration [16]. Using the PL signal outside the ring structures, the dopant-related base resistivity of an as-cut wafer can be determined although TD are present (see marked areas in Fig. 6).

3.2 Calibration of the PL signal to base resistivity

For the calibration of the PL signal to base resistivity, the surface morphology of the as-cut wafers and the dopant type has to be considered, since the PL signal depends on the PL setup, the reflection of the surface, the dopant concentration and the free carrier concentration. For the calibration of the PL-BR method within this paper, the same p-type and n-type wafers from section 2.2 are used.

The calibration for p-type Cz-Si was done with Cz-Si samples with different dopant concentrations and without TD in the as-cut state (red squares in Fig. 2). Since for the n-type Cz-Si less wafers without TD were available, additional wafers with TD from group 2 from section 2.2 were taken. These calibration samples had a rough surface in the as-cut state. For the calibration the mean values and standard deviations of the corner area (red marks in Fig. 6) were taken. All determined PL signals were corrected for background signal. In addition, the mean values and standard deviations of the base resistivity line scan were determined from four-point probe measurement of the whole Cz-Si wafer. In Fig. 7 such determined PL signals are plotted against the related base resistivities for both kinds of doping. The lines display the correlation between both values by $I_{PL}=A*\rho^b$ with the fit parameters A and b.

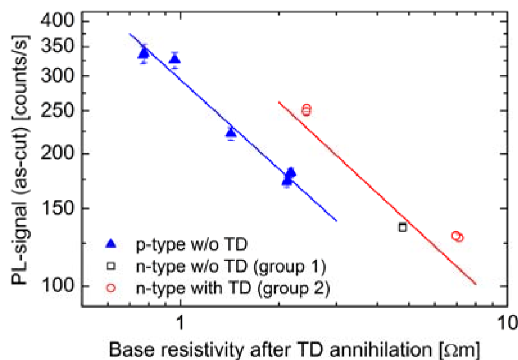

Fig. 7. Mean PL signal and standard deviation of the corner areas plotted against the corresponding mean base resistivity together with the standard deviation of the whole wafer after thermal donor annihilation of the p-type calibration wafers (blue symbols) and the n-type calibration wafers (red and black symbols).

3.3 Proof of principle of the PL-BR method

Using the calibration curves from section 3.2, the PL signals averaged over the corner areas of each wafer from section 2.2 are converted into base resistivities. These calculated values of the base resistivities are compared with the mean value of the four-point-probe measurement after TD annihilation. The comparison is shown for the investigated p- and n-type silicon in Fig. 8.

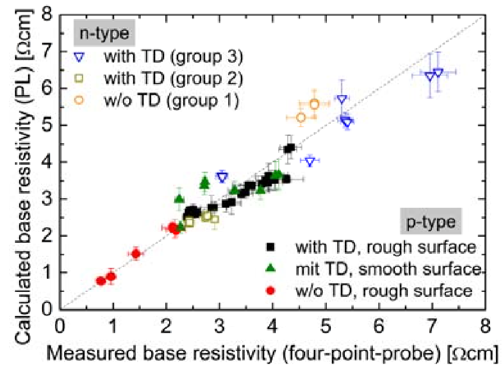

Fig. 8. Comparison of the calculated base resistivity from the PL signal with the via four-point-probe measurement determined value. The p-type silicon is displayed with closed symbols and the n-type silicon with open symbols. The dotted line is a bisecting line for orientation.

For p-type silicon, the calculated base resistivity values of the samples with a rough surface are in good agreement with the measured ones. Below a base resistivity of 3.5 Ωcm the deviation of the prediction is 0.3 Ωcm from the measured value and the highest deviation with a value of 0.5 Ωcm was measured for a wafer with a base resistivity of > 4 Ωcm. As expected, due to the different surface, the absolute deviation is higher for the wafers with a smooth (diamond cut) surface, the highest deviation for this kind of samples was determined with 0.8 Ωcm. For n-type silicon the calculated base resistivity values from the as-cut PL image seems to be less accurate than the prediction for the p-type silicon. The highest absolute deviation is 0.8 Ωcm, although the surface of all wafers was similar. In contrast to the p-type Si the base resistivity of the n-type samples is higher.

Table I gives an overview on the observed relative deviations of the investigated p-type and n-type silicon. In addition, the threshold deviation to calculate an emitter with 120 Ω/sq with an error less than 5 % for a sample with 180 µm thickness is listed. For each base resistivity range, the maximal value of the deviation is given. The numbers in brackets indicates how many of the samples of the group match the 5 % limit.

For the investigated p-type Cz-silicon with a rough surface and base resistivities higher than 3 Ωcm, the determination of the dopant-related base resistivity in the as-cut state with the PL-BR method is as accurate as needed to calculate the emitter within an error of 5 %. For samples with a base resistivity between 1 Ωcm and 2 Ωcm, half of the samples are within the 5 % limit of the emitter deviation value. For the investigated n-type Cz-silicon 13 of the 17 samples are within the 5 % limit of the emitter deviation, and especially 6 of the 7 samples, which were not used for the calibration, fulfill the limit. Therefore also for both p-type and n-type silicon the PL-BR method works well for base resistivity determination.

As can be seen from Fig. 9, the deviations of the base resistivity determination are smaller with the PL-BR method than the one due to uncorrected thermal donors.

Table I: Maximal deviation of the PL determined base resistivity from the measured base resistivity by four-point probe measurements for p-type and n-type samples. The second column shows the highest deviation value which is acceptable so that the deviation of the emitter value is less than 5%. The numbers in brackets indicate how many of the samples of the group match the 5 % limit.

Base resistivity	5% emitter limit[3]	P-type: rough surface	P-type: smooth surface	N-type: w/o TD (group 1)	N-type: with TD (group 2)	N-type: with TD (group 3)
0-1 Ωcm	4.2 %	7.2 % (2/4)	---	---	---	---
1-2 Ωcm	8.1 %	9.1 % (1/2)	---	---	---	---
2-3 Ωcm	11.6 %	13.9 % (13/16)	37.8 % (1/4)	---	3.6 % (2/2)	15.8 % (2/3)
3-4 Ωcm	14.9 %	10.1 % (11/11)	1.5 % (2/2)	---	---	19.5 % (0/2)
4-5 Ωcm	18.0 %	12.8 % (4/4)	5.1 % (2/2)	17.3 % (2/3)	---	13.9 % (1/1)
5-6 Ωcm	20.9 %	---	---	---	8.2 % (1/1)	5.8 % (2/2)
> 6 Ωcm	>20.9 %	---	---	---	9.6 % (2/2)	4.4 % (1/1)

[3] From Fig. 4, valid for a 120 Ω/sq Emitter and a wafer thickness of 180 μm

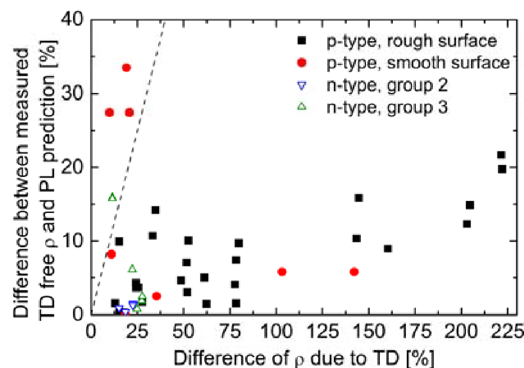

Fig. 9. Comparison of the differences of the as-cut base resistivity values measured by inductive measurement (large deviation) or PL (small deviation) with the TD free base resistivity.

4 SUMMARY

If thermal donors are present in Cz-Si as-cut wafers, the results of inductive base resistivity measurements get strongly distorted so that accurate emitter sheet resistivity calculation are not possible anymore. Therefore, a new method to determine the dopant-related base resistivity despite the presence of thermal donors was developed to overcome this measurement problem. It could be shown that the predicted values by the PL-BR method fit well with the base resistivity values measured after annihilation of the thermal donors. Furthermore, it was demonstrated that the base resistivity determination with PL-BR is as accurate as needed for the calculation of the emitter sheet resistivity for 85 % of the investigated p-type (<1 Ωcm) and for 100 % of the investigated n-type samples. Since this method requires only a single PL-image and can be performed in the as-cut state without further treatment it can be used to improve incoming inspection and emitter quality control.

5 ACKNOWLEDGEMENT

This work has been internally supported by the Fraunhofer Society and by the German Federal Ministry for for Economic Affairs and Energy within the research project “THESSO” under contract number 0325491.

6 REFERENCES

[1] U. Gösele and T. Y. Tan, "Oxygen diffusion and thermal donor formation in silicon," *Applied Physics A,* vol. 28, pp. 79-92, 1982.

[2] R. C. Newman, "Thermal donors in silicon: oxygen clusters or self-interstitial aggregates," *Journal of Physics C: Solid State Physics,* vol. 18, pp. 967-972, 1985.

[3] A. Ourmazd, *et al.*, "Oxygen-related thermal donors in silicon: A new structural and kinetic model," *Journal of Applied Physics,* vol. 56, pp. 1670-1681, 1984.

[4] J. Veirman, *et al.*, "A Fast and Easily Implemented Method for Interstitial Oxygen Concentration Mapping Through the Activation of Thermal Donors in Silicon," *Energy Procedia,* vol. 8, pp. 41-46, 2011.

[5] V. V. Voronkov, "Generation of thermal donors in silicon: oxygen aggregation controled by self-interstitials," *Semicond. Sci. Technol.,* vol. 8, pp. 2037-2047, 1993.

[6] M. Spitz, *et al.*, "Fast inductive inline measurement of the emitter sheet resistance in industrial solar cell fabrication," in *Proceedings of the 22nd European Photovoltaic Solar Energy Conference*, Milan, Italy, 2007, pp. 47-50.

[7] J. Haunschild, *et al.*, "Quality control of czochralski grown silicon wafers in solar cell production using photoluminescence imaging," in *Proceedings of the 26th European Photovoltaic Solar Energy Conference and Exhibition*, Hamburg, Germany, 2011, pp. 1025-1030.

[8] P. Wagner and J. Hage, "Thermal Double Donors in Silicon," *Appl. Phys. A,* vol. 49, pp. 123-138, 1989.

[9] W. Götz, *et al.*, "Thermal donor formation and annihilation at temperatures above 500 °C in Czochralski-grown Si," *Journal of Applied Physics,* vol. 84, pp. 3561-3568, 1998.

[10] L. I. Murin, *et al.*, "Thermal double donor annihilation and oxygen precipitation at around 650 °C in Czochralski-grown Si: local vibrational mode studies," *Journal of Physics: Condensed Matter,* vol. 17, p. S2237, 2005.

[11] Y. Tokuda, *et al.*, "Thermal donor annihilation and defect production in n-type silicon by rapid thermal annealing," *Journal of Applied Physics,* vol. 66, pp. 3651-3655, 1989.

[12] D. Biro, *et al.*, "PV-Tec: Photovoltaic technology evaluation center - design and implementation of a production research unit," in *Proceedings of the 21st European Photovoltaic Solar Energy Conference*, Dresden, Germany, 2006, pp. 621-624.

[13] M. Kirpo, "Global simulation of the Czochralski silicon crystal growth in ANSYS FLUENT," *Journal of Crystal Growth,* vol. 371, pp. 60-69, 2013.

[14] A. Sabanskis, *et al.*, "Crystal shape 2D modeling for transient CZ silicon crystal growth," *Journal of Crystal Growth,* vol. 377, pp. 9-16, 2013.

[15] J. Haunschild, *Lumineszenz-Imaging - vom Block zum Modul*: Fraunhofer-Verlag, 2012.

[16] T. Trupke and R. A. Bardos, "Photoluminescence: a surprisingly sensitive lifetime technique," in *Proceedings of the 31st IEEE Photovoltaic Specialists Conference*, Orlando, Florida, USA, 2005, pp. 903-906.